DOI: 10.1161/CIRCEP.113.000404

# Sinoatrial Node Reentry in a Canine Chronic Left Ventricular Infarct Model: The Role of Intranodal Fibrosis and Heterogeneity of Refractoriness

**Running title:** *Glukhov et al.; Sinoatrial Node Reentry*

Alexey V. Glukhov, PhD[1]; Lori T. Hage, BSc[1]; Brian J. Hansen[1]; Adriana Pedraza-Toscano, DVM, PhD[2]; Pedro Vargas-Pinto, DVM, PhD[2]; Robert L. Hamlin, DVM, PhD[2]; Raul Weiss, MD, FAHA, FHRS[3]; Cynthia A. Carnes, PharmD, PhD, FAHA, FHRS[1,4]; George E. Billman, PhD, FAHA, FHRS[1]; Vadim V. Fedorov, PhD[1,4]

[1]Department of Physiology & Cell Biology, [2]College of Veterinary Medicine, [3]Division of Cardiovascular Medicine, [4] College of Pharmacy, College of Medicine, Dorothy M. Davis Heart and Lung Research Institute, Ohio State University, Columbus, OH

**Correspondence:**

Vadim V. Fedorov, PhD

Department of Physiology and Cell Biology

College of Medicine, The Ohio State University

306 Hamilton Hall, 1645 Neil Avenue

Columbus, OH 43210-1218

Tel: 1-614-292-5154

Fax: 1-614-292-4888

E-mails: vadim.fedorov@osumc.edu / fedorov.2@osu.edu

**Journal Subject Codes:** [130] Animal models of human disease, [132] Arrythmias-basic studies

DOI: 10.1161/CIRCEP.113.000404

**Abstract:**

***Background -*** Reentrant arrhythmias involving the sinoatrial node (SAN), namely, SAN reentry, remain one of the most intriguing enigmas of cardiac electrophysiology. The goal of the present study was to elucidate the mechanism of SAN micro-reentry in canine hearts with post myocardial infarction (MI) structural remodeling.

***Methods and Results -*** In vivo, Holter monitoring revealed ventricular arrhythmias and SAN dysfunctions in post left ventricular MI (6-15 wks) dogs (n=5) compared to control dogs (n=4). In vitro, high resolution near-infrared optical mapping of intramural SAN activation was performed in coronary perfused atrial preparations from MI (n=5) and controls (n=4). Both SAN macro- (slow-fast; 16-28 mm) and micro-reentries (1-3 mm) were observed in 60% of the MI preparations during moderate autonomic stimulation (acetylcholine (0.1 μM) or isoproterenol (0.01-0.1 μM)) after termination of atrial tachypacing (5-8 Hz), a finding not seen in controls. The autonomic stimulation induced heterogeneous changes in the SAN refractoriness; thus, competing atrial and/or SAN pacemaker waves could produce unidirectional blocks and initiate intranodal micro-reentries. The micro-reentry pivot waves were anchored to the longitudinal block region and produced both tachycardia and paradoxical bradycardia (due to exit block), despite an atrial ECG morphology identical to regular sinus rhythm. Intranodal longitudinal conduction blocks coincided with interstitial fibrosis strands that were exaggerated in the MI SAN pacemaker complex (fibrosis density 37±7% MI vs. 23±6% control, P<0.001).

***Conclusions -*** Both tachy- and bradyarrhythmias can result from SAN micro-reentries. Post-infarction remodeling, including increased intranodal fibrosis and heterogeneity of refractoriness, provides substrates for SAN reentry.

**Key words:** sinoatrial node; sinoatrial node reentry; autonomic stimulation; optical mapping; myocardial infarction

DOI: 10.1161/CIRCEP.113.000404

## Introduction

Sinus nodal reentrant tachycardia, also called "SAN reentry", is a reentrant tachyarrhythmia involving the SAN and/or perinodal tissue.[1, 2] SAN reentrant tachycardia may account for 2–17% of all arrhythmias;[2-5] nonetheless, its underlying mechanisms are still poorly understood. However, SAN reentry arrhythmias are difficult to diagnose due to electrocardiographic similarity of the P-wave to the normal sinus rhythm.[1] Since it is practically impossible to record the electrical activity of the human SAN directly in vivo, the clinical diagnosis of SAN reentry is based solely on indirect evidence such as P-wave morphology, configuration of atrial electrograms, or initiation and termination of sinus arrhythmia paroxysms by burst stimulation.[2]

In 1943, Barker et al.[6] were the first to propose that reentry could occur within the SAN. Utilizing a single microelectrode technique on an isolated rabbit heart, Han et al.[7] in 1968 demonstrated functional conduction dissociation within the SAN after introduction of a premature atrial beat. In 1979, the first and only direct demonstration of a single SAN reentrant echo beat, in only one rabbit heart, was reported by Allessie and Bonke via consecutive single microelectrode mapping.[8] Notably, more than 30 years later, the anatomical and electrophysiological determinants of SAN reentry are poorly elucidated due to the lack of direct mapping data. Patients with SAN reentrant tachycardia have a high incidence of concurrent structural heart diseases including valvular disease, coronary artery disease, or hypertensive heart disease.[3, 4] These findings suggest that structural and/or functional remodeling of specialized conduction structures, such as the pacemaker complex, could alter conduction properties and form the substrate necessary for SAN reentry. Therefore, to test our hypothesis that structural remodeling promotes the induction of SAN reentry, we used a well-established canine model of post (6-15 weeks) left ventricular infarction (MI, left anterior descending artery ligation).

DOI: 10.1161/CIRCEP.113.000404

Currently, optical mapping of an isolated heart is the only available technique[9, 10] that provides detailed measurements of dynamic activation of complex three-dimensional structures, such as the SAN.[11] Recently, we combined multi-structural near-infrared fluorescence optical mapping with analytical signal processing to unmask and to resolve the intramural activation and repolarization patterns of the canine SAN from the intervening atrial epicardial and endocardial layers.[12] In this report, we present the first instance of near-infrared fluorescence optical mapping of micro-reentry (1-3 mm size) within the canine SAN pacemaker complex.

**Methods**

All animal procedures and protocols were approved by the Ohio State University Institutional Animal Care and Use Committee. An expanded Methods section is available in the supplemental methods section in the online-only Data Supplement.

We studied a canine model of post (6-15 weeks) left ventricular infarction (MI, left anterior descending artery ligation) that exhibits in vivo heart rhythm alternations (**Figure 1 and Supplement Figure 1**) due to structural remodeling and autonomic imbalance[13] (n=10). Normal dogs of similar age and weight (n=8) served as a control group for functional and structural data. A Holter monitor was placed on the dogs (5 MI and 4 Control) with a 2 lead system with electrodes in a standard precordial placement. Optical mapping of the canine SAN has been previously described.[14, 15] a rate of 1,000 frames/sec with the MiCam Ultima-L CMOS camera (SciMedia, Costa Mesa, CA) with an optical field of view of 25x25 mm (250 μm/pixel) using the excitation-contraction uncoupler blebbistatin[16] (10-20 μM, Tocris Biosciences, Ellisville, MO) and the near-infrared voltage-sensitive dye, di-4-ANBDQBS[17] (10-40 μM). The anatomical location of the SAN pacemaker complex and its specialized sinoatrial conduction pathways

(SACPs) were identified via histology and immunolabeling of connexin 43 (**Figure 2A**) as recently described in our laboratory.[12, 15]

***Statistics***

Quantitative data are shown as mean ± SD. Hypothesis testing was performed using an unpaired Student's t-test or non-parametric Mann-Whitney test (Minitab 16) dependent on normality assumptions which were tested using Anderson-Darling test. The significance of between-group SAN reentry incidence was tested between MI and control animals using Fisher's exact test in SAS 9.2. A $P<0.05$ was considered to be statistically significant.



**Results**

***SAN dysfunctions observed in vivo***

The MI dogs repeatedly exhibited in vivo evidence of apparent SAN dysfunctions (**Figure 1**) including SAN bradycardia and atrial pauses. Maximum atrial pauses were significantly prolonged in MI dogs compared with controls (3.6±0.9 s versus 1.6±0.2 s respectively, P=0.020). In MI dogs, these pauses were often obtained after termination of either ventricular or supraventricular tachyarrhythmias (**Supplement Figure 2**). Atrial pauses in MI dogs could also be repeatedly elicited during episodes of tachy-brady arrhythmias with the same ECG P-wave morphology as seen in normal sinus rhythm (**Figure 1 and Supplement Figure 1**).



***Structural and functional remodeling of the SAN in MI dogs***

Histological evaluation[14] of the SAN pacemaker complex (**Figure 2**) revealed a significant increase in intranodal fibrosis in the post MI as compared with control dogs (37±7% MI vs. 23±6% control fibrosis density, P<0.001). Functionally, the SAN region was defined from the morphology of optical action potentials (OAPs) according to two criteria: presence of slow diastolic depolarization and upstrokes with multiple components corresponding to activation in

different layers of conduction (**Figure 2B**, OAPs traces: blue recording).[10, 14] Double upstrokes of OAPs were then used to reconstruct two separate activation patterns: "*slow SAN*" excitation from the leading pacemaker (**Figure 2B**, middle activation map) and "*fast atrial*" excitation originating from the SACPs (**Figure 2B**, right activation map). *In vitro*, at baseline, moderate sinus bradycardia and slightly prolonged SAN conduction times were observed in MI preparations compared with controls (sinus cycle length: 550±41ms versus 477±49ms, *P*=0.031; and SAN conduction time: 58±13ms versus 41±15ms, *P*=0.023).

***SAN reentry induced by atrial tachypacing and autonomic stimulation***

Different forms of SAN dysfunctions including intranodal reentry were provoked by atrial tachypacing (5Hz and higher) (**Figures 3-8, and Supplement Figures 3-5 and Movies 1-4**). Slow (3.3 Hz) atrial pacing was not sufficient to provoke SAN dysfunctions (data not shown). This observation confirms our recent studies,[12, 15, 18] which demonstrated that only atrial tachypacing can significantly depress conduction within normal canine hearts and produce both entrance and exit SAN blocks.



At baseline, atrial tachypacing (7.5Hz) induced exit blocks in two MI but not in control dog hearts (**Figure 3A**). After application of acetylcholine (ACh), atrial tachypacing induced both brady- and tachy-arrhythmias, including SAN exit block, atrial flutter and atrial fibrillation (**Figure 3B-C**). Although SAN exit block and atrial flutter/fibrillation were observed in control canine hearts during ACh (0.3-1 μM), no SAN reentrant arrhythmias were revealed in these hearts in agreement with our previous studies.[15] Notably, in contrast to control hearts, during exposure to tachypacing under autonomic stimulation, three out of five MI preparations exhibited SAN reentry paroxysms (1-9 sec, 2-21 reentry beats) manifested by both atrial tachycardia and paradoxical bradycardia on the ECG (tachy-brady arrhythmias), similar to those

observed *in vivo*. This finding was not seen in normal canine preparations in either the present study (p=0.025, MI (3 out of 5) vs. control (0 out of 4)) or in previous studies (0 out of 17 in animals).[12, 15]

When optically mapped, these dysfunctions were characterized by reentrant movement of the excitation wave within the SAN. We found several forms of reentry associated with the SAN: (1) macro-reentry involving excitation wave propagation from the SAN (slow reentry pathway, 6-8 mm) to atria (fast reentry pathway, 10-20 mm) and back to SAN (SAN total slow-fast reentry pathway, 16-28 mm); and both (2) counter- and (3) clockwise micro-reentries inside the SAN (SAN intranodal micro-reentry pathway, 1-3 mm) (**Figure 4 and Supplement Figure 3**). After atrial tachypacing, the SAN was activated by the atria through the left superior SACP which then repeatedly re-activated the atria through the right superior SACP (**Figure 4, panel R1, Supplement Figure 3 and Movie 1**). After two consecutive macro-reentrant beats, the propagation in SACPs was blocked and macro-reentry transformed into a sustained counterclockwise micro-reentry within the SAN (**Figure 4 panel R2**). The SAN activation map revealed longitudinal dissociation of intranodal conduction in the superior SAN compartment as well as transverse bidirectional block in the inferior SAN compartment (**Supplement Figure 4 and Movie 2**). Subsequent activation of the pacemaker located in the inferior SAN compartment led to competition between the pacemaker and the micro-reentry circuit that, in turn, resulted in a change of direction of the micro-reentry circuit from counter-clockwise to clockwise (**Figure 4, panel R3**). After four successive beats, reentry was blocked in the right part of the superior SAN compartment. Thus, the pacemaker cluster located in the right part of the SAN head was not paced by the reentrant wave and thereby became a leading pacemaker for the first sinus beat.

Termination of SAN reentry led to a slight slowing of atrial rhythm without changes in

ECG morphology.

Another example of two forms of SAN reentry registered in MI canine heart #1 is shown in **Supplement Figure 5**. In this dog, both slow-fast SAN macro- and micro-reentries were observed during perfusion with 0.01 μM Iso. In MI canine #2, non-sustained slow-fast SAN reentry (2-5 beats) was registered during 0.1 μM Iso perfusion (not shown).

***Heterogeneous refractoriness as the mechanism of SAN reentry***

To define the exact mechanism of SAN reentry initiation during atrial tachypacing, dominant frequency (DF) analysis (**Figure 5A**) was applied.[12, 15] We used DF analysis as a surrogate for refractoriness (**Figure 5B**) allowing us to assess the heterogeneity within the SAN complex and correlate it with vulnerability to SAN reentry in accordance with the classical view on reentry initiation.[19]

In the MI heart #3, SAN micro-reentries were induced only during 0.1 μM ACh or after washout of ACh followed by 0.01 and 0.1 μM Iso (**Figure 5**). The SAN micro-reentries could not be induced in the same heart even with higher concentrations of ACh (0.3 and 1 μM), at baseline, or after washout of ACh prior to application of Iso. At baseline, the MI SAN complex was paced by atrial waves preferentially from inferior SACPs as previously shown for control dogs.[12, 14, 15] Atrial waves first entered the SAN tail compartment and slowly propagated to the SAN head with periodic entrance blocks between all three main compartments. As such, the SAN tail (red OAP #3) was more frequently paced (the fastest DF within the SAN) than the SAN head (blue OAP#1) (the slowest DF within the SAN). Moderate cholinergic stimulation (ACh 0.1 μM) heterogeneously affected the refractoriness and conduction of these SAN compartments. DF analysis revealed shortening of refractoriness near the right superior SACP (pink OAP #4, the fastest DF within the SAN) and an increase in refractoriness of other SAN compartments

(blue OAP # 1, the slowest DF within the SAN) (**Figure 5** for ACh 0.1 μM). Therefore, the SAN was preferentially paced from the right superior SACP that formed a longitudinal unidirectional conduction block due to heterogeneous refractoriness of the left and right parts of the SAN head and center compartments. Importantly, the tachypacing-induced intranodal conduction block between the left and right parts of SAN compartments, was not observed in normal canine preparations either in the present study (n=4) or in our previous studies (n=17).[12, 15]

Interestingly, higher doses of ACh (0.3-1 uM) significantly depressed excitability near SACPs and homogenized differences in functional refractoriness between the SAN compartments. It prevented an induction of longitudinal conduction dissociation and thus SAN reentry (**Figure 5** for ACh 0.3 μM, and **Figure 3C** for ACh 1 μM). Only exit and entrance SAN blocks could be observed during these conditions (**Figure 3**).

Washout of ACh and then an application of Iso (0.01 μM) heterogeneously increased intranodal conduction and shortened the refractoriness within the SAN compartments. DF analysis revealed significant shortening of refractoriness in the right superior SACP and in the SAN tail, and no changes observed in the left part of the SAN head compartment. This dispersion of refractoriness also led to the longitudinal conduction block within both SAN head and center during atrial tachypacing (**Figure 5** for Iso 0.01 μM).

**Figure 6** shows complete patterns of reproducible intranodal SAN micro-reentries that occurred in the MI canine heart #3 within 10s of cessation of atrial tachypacing during ACh 0.1 μM (see also **Supplement Movie 3**). To more precisely analyze the SAN activation pattern during atrial tachypacing, the SAN OAP extraction algorithm was applied to remove atrial components from SAN OAPs as described recently[12] (see also **Figure 2D**). Atrial tachypacing depressed longitudinal intranodal conduction and thus led to unidirectional longitudinal block and

clockwise reentry (cycle length: 487±14 ms). Corresponding histological analysis revealed that the longitudinal intranodal block correlated with fibrosis strands thereby forming a structural substrate for SAN reentry (**Figure 6A**).

During Iso 0.01 μM perfusion, the longitudinal conduction block again served as a main substrate for initiation of SAN slow-fast macro-reentry which then transformed into SAN intranodal micro-reentry (**Figure 7 and Movie 4**). Micro-reentry pivot circuits were anchored to the area of longitudinal conduction block and could produce both atrial tachycardia and paradoxical bradycardia (due to transient exit block), despite an atrial ECG morphology identical to that seen during regular sinus rhythm. It should be noted that on average (n=5 reentry paroxysms during Iso 0.01 μM perfusion), SAN reentry cycle length was slightly faster than that of sinus rhythm after reentry termination (378±18 ms vs. 410±11 ms, P=0.001).

In all three MI preparations where SAN micro-reentries were induced, both tachycardia and paradoxical bradycardia were observed due to transient SAN exit block, even during Iso applications (**Figures 4, 6-8, and Supplement Figures 3-5**). **Figure 8** shows that the mechanism of the SAN exit block that occurred during reentry was related to the diminished electrical current delivered through SACPs to the atrium. The diminished current was evident from the low OAP amplitudes and derivatives ($dV/dt_{max}$) recorded from the SAN and SACPs during reentry (the same example as that in **Figure 6**). **Figure 8B** demonstrates that during reentry, $dV/dt_{max}$ values near the SACP were significantly diminished when compared with atrial waves or normal SAN waves. Similarly, **Figure 7D** shows that alternations of $dV/dt_{max}$ in SACPs occurring during SAN micro-reentry led to the transient exit block.

## Discussion

This study is the first direct demonstration of SAN micro-reentry (1-3 mm), as a consequence of

structural heart disease; a possibility that has been hypothesized for decades but has never been directly observed previously. We report that the mechanism underlying canine SAN reentry induction is likely associated with an enhanced heterogeneity of refractoriness within the SAN compartments conditioned by autonomic stimulation and in part by strands of increased interstitial fibrosis due to post MI remodeling.

***SAN refractoriness***

Only a few studies have reported SAN refractoriness measurements. Indirect clinical measurements of SAN refractoriness demonstrated that they can be significantly affected by autonomic stimulation, especially in patients with SAN dysfunctions.[20] Similarly to AVN cells,[21] refractoriness of primary SAN pacemaker cells[22] depends on the slow upstroke $I_{Ca,L}$ current. Thus, action potential duration (APD) does not always determine refractoriness of pacemaker cells because of the presence of post-repolarization refractoriness in the SAN, exaggerated by autonomic stimulation as shown previously by Prystowsky et al. (1979).[23] The authors observed that the functional refractory period of the SAN central compartment exceeds APD by ~18% at baseline and by ~25% after 0.5 μM ACh with complete dissociation between refractoriness and APD after 5 μM ACh due to entrance block to the SAN. Our own APD analysis showed similar dissociation between APD and functional local refractoriness measured by DF methods (compare **Figure 5 and Supplement Figure 6**). Thus, we used DF as an indicator of the minimal pacing interval which could be captured by the atrial myocardium and SAN compartments during tachypacing which is determined by the local functional refractoriness of the tissue.[15, 24] We suggest that DF analysis of SAN activation during tachypacing could provide a more direct pattern of SAN complex refractoriness than SAN repolarization maps. During tachypacing, multiple atrial waves attempted to enter the SAN complex through different SACPs, which due

to different conduction filtering properties of the SACPs[12, 15] resulted in multiple wave collisions inside of the SAN compartments. Eventually, we were able to get an average of the minimal activation interval (which we defined as functional refractory period) which could be captured by each SAN compartment during atrial tachypacing by analyzing 8-16 second optical recordings with the DF method. It also should be noted that the minimal pacing interval rather than effective refractory period measured by S1-S2 protocol is similar to the rate of intramyocardial reentry.[25, 26] The SAN micro-reentry cycle length measurements support these suggestions as they were very close to functional refractoriness values near the reentry cores. As shown in **Figure 5**, SAN refractoriness at 0.1 μM ACh was 498±21 ms (left head) and 443±51 ms (center) which was very close to the cycle length of 487±14 ms for the SAN micro-reentry in this area (**Figure 6**). At 0.01 μM Iso, SAN refractoriness was 391±15 ms (left head) and 345±16 ms (center) which also was very close to the SAN micro-reentry cycle length of 378±18 ms (**Figure 7**).



Previously, we demonstrated in healthy canine SAN that during tachypacing SAN compartments exhibit differential functional refractoriness that can be heterogeneously increased by ACh or adenosine or decreased by Iso.[12, 15] The microelectrode rabbit SAN study,[23] showed that ACh could prolong refractoriness within the SAN center but shorten it in the SAN periphery near the crista terminals border. Our previous modeling study of single SAN pacemaker cell excitability showed[22] a nonmonotonous dependence of the excitation threshold (by external stimulus) on ACh concentration due to depression of the upstroke $I_{Ca,L}$ current, and hyperpolarization and action potential shortening due to $I_{K(ACh)}$ activation. We suggest that low ACh concentrations can shorten refractoriness exclusively near the SACPs where the influence of hyperpolarization from the atrial myocardium is more significant (**Figure 5**, **ACh 0.1 μM**). Higher ACh concentrations would lead to greater depression of $I_{Ca,L}$ and excitability which

already increased refractoriness of the SACPs and depressed conduction in the entire SAN pacemaker complex (**Figure 5, ACh 0.3 μM**).

***Substrate for SAN reentry: intranodal conduction block and heterogeneous refractoriness***

Classically, initiation of reentry requires a trigger (extra beat) and a substrate (heterogeneity refractoriness and/or conduction abnormalities) leading to unidirectional block.[24] Despite the very heterogeneous structure of the healthy SAN complex[8, 23, 27] characterized by significant gradients of repolarization and refractoriness as well as slow and anisotropic conduction, it is practically impossible to induce SAN reentry in normal hearts. High physiological dispersion of SAN refractoriness and conduction at baseline and during autonomic stimulation do not lead to SAN reentry in healthy rabbit[23] or dog hearts,[12, 15] except for single SAN reentrant echo beats.[8] In the present study, SAN reentry occurred exclusively in the diseased canine hearts characterized by enhanced intranodal fibrosis compared to healthy hearts.[12, 15] Support for the role of structural heart disease in arrhythmogenesis was also evident in our recent work where we could induce atrio-ventricular nodal reentry in explanted failing human heart preparations during autonomic stimulation, due to longitudinal conduction dissociation in the compact node.[13]



**Figures 5-7** show that both longitudinal (from SAN head to tail) and transverse (from the right to left SAN borders) gradients in refractoriness within the SAN compartments resulted in unidirectional, intranodal conduction block. Subsequent SAN reentry induction was conditioned by moderate autonomic stimulations and strands of increased interstitial fibrosis (**Figures 5-7**). Thus, we hypothesize that MI-induced intranodal fibrosis exaggerates the functional heterogeneity between the SAN compartments by diminishing electrotonic influence (mutual entrainments) and also serves as an additional structural substrate for reentry. Indeed, the size (1-3 mm) and the location of the SAN micro-reentrant circuits obtained were anatomically

determined by the strands of interstitial fibrosis (**Figures 6 and 7**).

The size of reentrant circuits observed in the present study is in agreement with the classical concept of wavelength for reentry: Wavelength = Refractoriness x Conduction Velocity.[28, 29] Our rough estimation of functional refractoriness by using DF measurements and conduction velocities in the region of SAN reentry circuits were in the range of 300-500 ms and 0.2-0.6 cm/sec respectively. It gives us a theoretical range for wavelength about 0.6-3 mm which is close to our experimentally observed reentry size of 1-3 mm.

***How can SAN reentry be induced?***



We demonstrate that in some cases atrial waves can directly initiate reentry by entering the SAN through one SACP, slowly rotating around the intranodal longitudinal block and then leaving the SAN through another SACP. In other cases, SAN reentry can occur during the first seconds of recovery from tachypacing during vagal and/or sympathetic stimulation. High dispersion of refractoriness within the SAN enables desynchronized firing of neighboring pacemaker compartments. Thus the earliest pacemaker activation wave can be blocked from propagating towards the neighboring compartment with longer refractoriness in the transverse direction but could propagate along the intranodal block. During the next 100-150 ms, recovery of the pacemaker compartment excitability in the compartment with longer refractoriness, would allow the wave to cross the longitudinal block and initiate SAN reentry. These mechanisms of SAN reentry initiation are supported by the classic studies of the Allessie group in which they demonstrated, using multi-electrode electrical mapping of isolated atria, that the induction of reentry by premature beats required spatial dispersion in refractory periods.[19]



***How can SAN macro- and micro-reentry be maintained and terminated?***

Depending on the excitable state of SACPs, two scenarios of reentry maintenance were

observed. First (*SAN macro-reentry*), the reentrant wave could propagate through an active SACP and then activate atrial myocardium. After 50 ms, the wave could re-excite another SAN compartment via another SACP and thus form a macro-reentry circuit with two main pathways: a slow path (6-8 mm) located inside the SAN (approximately 300-350 ms) and another fast pathway (10-20 mm) located outside of the SAN between two SACPs. *Second* (*SAN micro-reentry*), when conduction in SACPs are depressed, SAN reentrant waves can circulate inside of the SAN around a longitudinal functional block (1-3mm) slowly drifting along the structural block.

Spontaneous termination of SAN reentry could result from decremental propagation or lack of re-excitation in the transverse direction across the line of block which leads to termination of reentry with an immediate restoration of pacemaker activity. In some cases, pacemaker compartments located outside of the reentry contour (for instance, in the inferior compartment of the SAN tail) could recover from overdrive suppression and then collide with the reentrant waves and terminate SAN intranodal reentry.



***When can SAN reentry be induced?***

It was previously demonstrated that in this MI model, dogs exhibit *in vivo* heart rhythm alternations due to autonomic imbalance, and enhanced sensitivity of $\beta_2$-adrenergic receptors.[27, 30, 31] Our Holter monitoring data obtained from the MI dogs demonstrated atrial pauses up to 7 sec as well as transient tachy-brady arrhythmias which occurred at early morning and were provoked by either autonomic tone fluctuations or short paroxysms of ventricular tachycardia (**Supplement Figure 2**). The fluctuations of autonomic tone may increase heterogeneity of the SAN complex refractoriness and conduction[15, 32] as well as provoking either atrial ectopic beats[31] or ventricular tachycadias which could trigger SAN reentry. Importantly, during moderate vagal

activation alone, external premature beats are required for initiation of SAN reentry. In contrast, during increased sympathetic activation, SAN reentry could occur spontaneously due to either an asynchronously accelerated pacemaker activity in different compartments or from a shift of the leading pacemaker to the border of heterogeneous refractoriness between the SAN compartments. As we demonstrated above, these conditions can initiate unidirectional conduction block and reentry without external atrial ectopic waves (**Figures 6 and 7**).

***Paradoxical bradycardia and SAN reentry***

Our data also suggest that SAN reentry could be responsible for the paradoxical bradyarrhythmic effect of β-adrenergic stimulation reported in 7% of patients in a study of >700 patients presenting for electrophysiology study.[33] Specifically, in the present study, β-adrenergic stimulation provoked SAN intranodal micro-reentry (1-3 mm size) that induced atrial pauses, leading to apparently paradoxical bradycardia on the ECG. The mechanism responsible for transient exit blocks during SAN micro-reentries can be attributed to diminished electrical current delivered from the functionally dissociated SAN to the atria via SACPs[34] since all electrical SAN reentrant waves reach SACPs at an oblique angle, as clearly evident from activation maps on **Figures 4-8**. Diminished electrical current through SACPs could cause transient exit block due to source-sink mismatch conditions, even during improved intrinsic SAN excitability by Iso. In contrast, during normally originating SAN pacemaker activity, all activation waves have broader fronts perpendicular to SACP regions and thus provide higher electrical current compared with the oblique SAN reentry waves.

These observations are further supported by the recent computer simulations by Siuniaev and Aliev (2012) that focused on the mechanisms and conditions for maintenance of micro-reentry in the rabbit SAN.[35] The authors, in part, demonstrated a periodic exit block of activation

from the SAN to the atrium during SAN intranodal micro-reentry, which are qualitatively similar to our experimental observations (**Figure 7C**).

***Potential limitations***

There are still many unanswered questions on what exactly predisposes the SAN to reentrant arrhythmias, as well as how these arrhythmias originate spontaneously *in vivo*. In the present study, we did not conduct *in vivo* electrophysiological studies where we could provoke SAN re-entry by using clinical methods. All MI dogs experienced the same experimental procedures and we could not identify differences between dogs that were or were not susceptible to SAN reentry, due to limited animal numbers. Indeed, few hearts developed the SAN reentrant arrhythmias *in vitro*, thus the absolute applicability of our findings to human SAN dysfunction *in vivo* is not clear. Our study provides an initial description of the mechanism(s) that is/are responsible for reentrant arrhythmias in the SAN pacemaker complex. Future studies will focus on the various functional, structural and molecular mechanisms responsible for both SAN macro- and micro-reentrant arrhythmias in other large animal models as well as directly in human hearts.



**Acknowledgments:** We thank Dr. Stanislav Zakharkin for his help in statistical data analysis, Jeanne Green for technical assistance and Dr. Rubin Aliev for valuable suggestions and critical comments.

**Funding Sources:** Davis Heart and Lung Research Institute (VVF), and NIH grants R01 HL115580-01A (VVF), HL089836 (CAC) and HL086700 (GEB).

**Conflict of Interest Disclosures:** None.

**References:**

1. Gomes JA, Mehta D, Langan MN. Sinus node reentrant tachycardia. *Pacing Clin Electrophysiol.* 1995;18:1045-1057.

2. Cossu SF, Steinberg JS. Supraventricular tachyarrhythmias involving the sinus node: Clinical

and electrophysiologic characteristics. *Prog Cardiovasc Dis.* 1998;41:51-63.

3. Wu D, Amat-y-leon F, Denes P, Dhingra RC, Pietras RJ, Rosen KM. Demonstration of sustained sinus and atrial re-entry as a mechanism of paroxysmal supraventricular tachycardia. *Circulation*. 1975;51:234-243.

4. Gomes JA, Hariman RJ, Kang PS, Chowdry IH. Sustained symptomatic sinus node reentrant tachycardia: Incidence, clinical significance, electrophysiologic observations and the effects of antiarrhythmic agents. *J Am Coll Cardiol*. 1985;5:45-57.

5. Sanders WE, Jr., Sorrentino RA, Greenfield RA, Shenasa H, Hamer ME, Wharton JM. Catheter ablation of sinoatrial node reentrant tachycardia. *J Am Coll Cardiol*. 1994;23:926-934.

6. Barker PS, Wilson FN, Johnson FD. The mechanism of auricular paroxysmal tachycardia. *Am Heart J.* 1943;26:435-445.

7. Han J, Malozzi AM, Moe GK. Sino-atrial reciprocation in the isolated rabbit heart. *Circ Res*. 1968;22:355-362.

8. Allessie MA, Bonke FI. Direct demonstration of sinus node reentry in the rabbit heart. *Circ Res*. 1979;44:557-568.

9. Herron TJ, Lee P, Jalife J. Optical imaging of voltage and calcium in cardiac cells & tissues. *Circ Res*. 2012;110:609-623.

10. Fedorov VV, Glukhov AV, Chang R. Conduction barriers and pathways of the sinoatrial pacemaker complex: Their role in normal rhythm and atrial arrhythmias. *Am J Physiol Heart Circ Physiol*. 2012;302:H1773-1783.

11. Chandler NJ, Greener ID, Tellez JO, Inada S, Musa H, Molenaar P, Difrancesco D, Baruscotti M, Longhi R, Anderson RH, Billeter R, Sharma V, Sigg DC, Boyett MR, Dobrzynski H. Molecular architecture of the human sinus node: Insights into the function of the cardiac pacemaker. *Circulation*. 2009;119:1562-1575.

12. Lou Q, Glukhov AV, Hansen B, Hage L, Vargas-Pinto P, Billman GE, Carnes CA, Fedorov VV. Tachy-brady arrhythmias: The critical role of adenosine-induced sinoatrial conduction block in post-tachycardia pauses. *Heart Rhythm*. 2013;10:110-118.

13. Fedorov VV, Ambrosi CM, Kostecki G, Hucker WJ, Glukhov AV, Wuskell JP, Loew LM, Moazami N, Efimov IR. Anatomic localization and autonomic modulation of atrioventricular junctional rhythm in failing human hearts. *Circ Arrhythm Electrophysiol.* 2011;4:515-525.

14. Fedorov VV, Schuessler RB, Hemphill M, Ambrosi CM, Chang R, Voloshina AS, Brown K, Hucker WJ, Efimov IR. Structural and functional evidence for discrete exit pathways that connect the canine sinoatrial node and atria. *Circ Res*. 2009;104:915-923.

15. Fedorov VV, Chang R, Glukhov AV, Kostecki G, Janks D, Schuessler RB, Efimov IR. Complex interactions between the sinoatrial node and atrium during reentrant arrhythmias in the canine heart. *Circulation*. 2010;122:782-789.

16. Fedorov VV, Lozinsky IT, Sosunov EA, Anyukhovsky EP, Rosen MR, Balke CW, Efimov IR. Application of blebbistatin as an excitation-contraction uncoupler for electrophysiologic study of rat and rabbit hearts. *Heart Rhythm*. 2007;4:619-626.

17. Matiukas A, Mitrea BG, Qin M, Pertsov AM, Shvedko AG, Warren MD, Zaitsev AV, Wuskell JP, Wei MD, Watras J, Loew LM. Near-infrared voltage-sensitive fluorescent dyes optimized for optical mapping in blood-perfused myocardium. *Heart Rhythm*. 2007;4:1441-1451.

18. Fedorov VV, Glukhov AV, Chang R, Kostecki G, Aferol H, Hucker WJ, Wuskell JP, Loew LM, Schuessler RB, Moazami N, Efimov IR. Optical mapping of the isolated coronary-perfused human sinus node. *J Am Coll Cardiol*. 2010;56:1386-1394.

19. Allessie MA, Bonke FI, Schopman FJ. Circus movement in rabbit atrial muscle as a mechanism of tachycardia. Ii. The role of nonuniform recovery of excitability in the occurrence of unidirectional block, as studied with multiple microelectrodes. *Circ Res*. 1976;39:168-177.

20. Kerr CR, Strauss HC. The measurement of sinus node refractoriness in man. *Circulation*. 1983;68:1231-1237.

21. Workman AJ, Kane KA, Rankin AC. Ionic basis of a differential effect of adenosine on refractoriness in rabbit av nodal and atrial isolated myocytes. *Cardiovasc Res*. 1999;43:974-984.

22. Aliev RR, Fedorov VV, Rozenshtraukh LV. Study of the effect of acetylcholine on the excitability of true pacemaker cells of rabbit sinus node using computer simulation. *Dokl Biochem Biophys*. 2005;402:223-225.

23. Prystowsky EN, Grant AO, Wallace AG, Strauss HC. An analysis of the effects of acetylcholine on conduction and refractoriness in the rabbit sinus node. *Circ Res*. 1979;44:112-120.

24. Berenfeld O, Zaitsev AV, Mironov SF, Pertsov AM, Jalife J. Frequency-dependent breakdown of wave propagation into fibrillatory conduction across the pectinate muscle network in the isolated sheep right atrium. *Circ Res*. 2002;90:1173-1180.

25. Rensma PL, Allessie MA, Lammers WJ, Bonke FI, Schalij MJ. Length of excitation wave and susceptibility to reentrant atrial arrhythmias in normal conscious dogs. *Circ Res*. 1988;62:395-410.

26. Smeets JL, Allessie MA, Lammers WJ, Bonke FI, Hollen J. The wavelength of the cardiac impulse and reentrant arrhythmias in isolated rabbit atrium. The role of heart rate, autonomic transmitters, temperature, and potassium. *Circ Res*. 1986;58:96-108.

27. Miyauchi Y, Zhou S, Okuyama Y, Miyauchi M, Hayashi H, Hamabe A, Fishbein MC, Mandel WJ, Chen LS, Chen PS, Karagueuzian HS. Altered atrial electrical restitution and heterogeneous sympathetic hyperinnervation in hearts with chronic left ventricular myocardial infarction: Implications for atrial fibrillation. *Circulation*. 2003;108:360-366.

28. Allessie MA, Lammers WJEP, Bonke FIM, Hollen J. Experimental evaluation of moe's multiple wavelet hypothesis of atrial fibrillation. *In: Zipes DP, Jalife J, eds. Cardiac electrophysiology and arrhythmias. NY, Grune&Stratton*. 1985:265-274.

29. Wiener N, Rosenblueth A. The mathematical formulation of the problem of conduction of impulses in a network of connected excitable elements, specifically in cardiac muscle. *Arch Inst Cardiol Mex.* 1946;16:205-265.

30. Billman GE. A comprehensive review and analysis of 25 years of data from an in vivo canine model of sudden cardiac death: Implications for future anti-arrhythmic drug development. *Pharmacol Ther.* 2006;111:808-835.

31. Houle MS, Altschuld RA, Billman GE. Enhanced in vivo and in vitro contractile responses to beta(2)-adrenergic receptor stimulation in dogs susceptible to lethal arrhythmias. *J Appl Physiol*. 2001;91:1627-1637.

32. Sharifov OF, Fedorov VV, Beloshapko GG, Glukhov AV, Yushmanova AV, Rosenshtraukh LV. Roles of adrenergic and cholinergic stimulation in spontaneous atrial fibrillation in dogs. *J Am Coll Cardiol*. 2004;43:483-490.

33. Brembilla-Perrot B, Muhanna I, Nippert M, Popovic B, Beurrier D, Houriez P, Terrier de la Chaise A, Claudon O, Louis P, Abdelaal A, State S, Andronache M, Suty-Selton C. Paradoxical effect of isoprenaline infusion. *Europace.* 2005;7:621-627.

34. Delmar M, Jalife J, Michaels DC. Effects of changes in excitability and intercellular coupling on synchronization in the rabbit sino-atrial node. *J Physiol.* 1986;370:127-150.

35. Siuniaev RA, Aliev RR. Computer simulations of microreentry in the SAN. *Biofizika*. 2012;57:870-875.

**Figure Legends:**

**Figure 1.** Maximum atrial pauses obtained from non-anesthetized control **(A)** and post-MI **(B)** dogs *in vivo* at rest. ECG recordings demonstrate a significantly prolonged maximum atrial pause in post-MI dogs compared with that in control dogs. The MI dogs repeatedly exhibited

DOI: 10.1161/CIRCEP.113.000404

atrial pauses caused by either ventricular tachycardia (panel B, upper ECG recording) or by apparent "SAN block" (panel B, middle ECG recording) as well as tachy-brady arrhythmias (panel B, lower ECG recording). The latter two ECGs have the same morphology of ECG P-wave as seen in normal sinus rhythm.

**Figure 2.** Anatomic and functional definition of the MI canine SAN. **(A)** Anatomical reconstruction of MI canine SAN from dog #3. Left panel: Epicardial photograph of the coronary-perfused canine atria preparation with a 25 x 25 mm optical field of view. The SAN was characterized by both histological staining (middle panel) and negative immunolabeling of connexin43 (Cx43; right panel). **(B)** Model of SAN pacemaker complex. Enlarged epicardial view of 3-dimensional canine SAN model based on structural and functional data. The SAN (red) consists of three major pacemaker compartments (head, center, and tail) and is isolated from the surrounding atrium (green) by 3 bifurcating coronary arteries (blue) and fibrosis (purple). Note the strands of the interstitial fibrosis inside the SAN. The four yellow bundles show SAN conduction pathways (SACPs) that electrically connect the SAN to the atrium. **(C)** Optical mapping of the canine SAN pacemaker complex activation during regular sinus rhythm. Separated SAN and atrial activation maps demonstrate a continuous propagation of the impulse originating in the inferior compartment of the SAN (tail) which excited the atrial myocardium via the right inferior SACP (open orange arrow). The white oval shows the location of the leading pacemaker inside the SAN; the pink circle shows the location of superior atrial exit point from the SAN (the earliest atrial activation site). **(D)** Optical action potentials (OAPs) recorded from the center of the SAN (blue) and from the atrial exit point in CT (green). Black dots indicate locations of the corresponding $dVdt_{max}$ used to calculate sino-atrial conduction time

(SACT). Below, the actual SAN signal extracted from the SAN OAP is shown. The extraction algorithm was described previously.[15] At the bottom, the corresponding ECG recorded from the isolated atrial preparation is shown. For each beat, a corresponding cycle length (CL) is shown. CT – crista terminalis; SVC and IVC – superior and inferior vena cava; RAA – right atrial appendage; PV – pulmonary veins; IAS – interatrial septum; FP – fat pad; CL – cycle length.

**Figure 3.** Acetylcholine induced brady- and tachy- arrhythmias in a post-MI atrial preparation (dog #3). **(A)** SAN exit block induced by fast atrial pacing (7.5 Hz) during the post-pacing SAN recovery time during control conditions. The SAN OAP (blue, 1) was selected from the center of the SAN; the atrial OAP (green, 2) - from the RA free wall. On the right of the OAPs, activation maps reconstructed for SAN excitation during SAN exit block (E1) and for the consequent SAN excitation (S1) are shown. During SAN exit block, propagation through all four SACPs was blocked (closed orange arrows). At the first SAN activation propagation of the atria, the right superior SACP was functional. **(B)** ACh (0.3 μM) shifted the leading pacemaker superiorly within the SAN and exaggerated atrial pauses due to SAN exit block (5370ms vs. 1077ms). On the right of the OAPs, activation map reconstructions for the last SAN excitation during SAN exit block (E1) and for the consequent SAN excitation (S1) are shown. Similar to panel A, during SAN exit block, propagation through all four SACPs was blocked (closed orange arrows). At the first SAN activation propagation to the atria, the right superior SACP was functional. **(C)** ACh (1 μM) with fast atrial pacing (10 Hz) during SAN exit block induced atrial flutter (AFL). From left to right: OAPs and their frequency power spectrums selected from the SAN center (blue, 1), and RA free wall (green, 2); atrial activation map during AFL; SAN activation during AFL; and dominant frequency map during AFL. Solid line shows the AFL circuit. During AFL,

the SAN could be retrogradely activated by atria through the right superior SACP. Propagation through the other three SACPs was blocked in both directions. Abbreviations are the same as those in Figure 2.

**Figure 4.** Evidence of multiple reentrant circuits inside the post-MI canine SAN. Atrial pacing during 0.01 μM Iso perfusion induced multiple heart rate abnormalities characterized by irregular rhythm and profound pauses on the ECG. Optical mapping of the SAN revealed several forms of reentries associated with the SAN. Below the OAPs, these arrhythmias are shown in greater detail. The white circle indicates the location of the leading pacemaker inside the SAN (if present) while the pink circle indicates superior atrial breakthrough. Functional left superior SACP conducting retrogradely and right superior pathway conducting anterogradely are shown by open white or black arrows. During SAN reentry, inferior SACPs were blocked. Abbreviations are the same as those in Figure 2.



**Figure 5.** Dominant frequency (DF) analysis applied to the SAN subjected to atrial tachypacing (7.5 Hz) at control and during autonomic stimulation. **(A)** Representative intranodal activation maps with anatomical SAN model as well as DF distribution maps were reconstructed from the most susceptible to SAN reentry, MI preparation #3. Arrows show main excitation propagation directions in the SAN complex during pacing. On the right of the DF maps, a frequency power spectrum is shown from the selected SAN compartments as well as from the right atrium. RS-right superior SACP. Abbreviations are the same as those in Figure 2. **(B)** Refractoriness of the different SAN compartments during baseline conditions and autonomic stimulations (n=2-3 for each data point). Inversed DF frequencies from panel **A** were used as a surrogate for

refractoriness to assess the heterogeneity within the SAN complex and correlate it with vulnerability to SAN reentry.

**Figure 6.** Detailed reconstruction of functional and structural anatomy of the SAN micro-reentry induction during ACh 0.1 μM the post-MI canine SAN. **(A)** Longitudinal conduction block (LB) induced by atrial tachypacing on the border of different refractoriness within the SAN (see Figure 5 for ACh 0.1 μM). Atrial wave is blocked towards the SAN compartment with long refractoriness and propagates in transverse direction. Subsequent retrograde activation of the SAN compartment with prolonged refractoriness initiated intranodal reentry around the functional block zone. **(B)** Clockwise micro-reentry inside of the SAN during 0.1 μM ACh perfusion. SAN exit block induced by fast atrial pacing (7.5 Hz) during the post-pacing SAN recovery time. During SAN block, two successive clockwise micro-reentrant circuits were traced inside the SAN (SAN OAPs 1-8). **(C)** OAPs selected from the right superior SACP (P) and the SAN micro-reentry circuit (1-7) trace LB formation during atrial tachypacing (7.5Hz) as well as reentry initiation and its spontaneous termination after two successful circuits (R1 and R2). Abbreviations are the same as those in Figure 2.

**Figure 7.** Induction of a counter-clockwise micro-reentry inside of the SAN during 0.01 μM Iso perfusion. **(A)** Longitudinal conduction block (LB) induced by atrial tachypacing (5 Hz) on the border of different refractoriness within the SAN (see Figure 5 for Iso 0.01 μM) is shown similar to Figure 6A. **(B)** SAN fast-slow macro-reentry (R1) through the SAN occurred in the MI canine heart #3 within the 10 s after cassation of atrial tachypacing is shown (see also Movie 4). **(C)** SAN slow-slow micro-reentry (R2) transformed from the previous macro-reentry is shown. **(D)**

DOI: 10.1161/CIRCEP.113.000404

OAPs selected from the right superior SACP (P) and the SAN micro-reentry circuit (1-4) trace LB formation as well as macro- and micro-reentry formation and spontaneous termination. Size and location of the reentrant circuits were determined by histological examination. During different reentry episodes (1-8 sec), the atrial myocardium was activated via the same SAN conduction pathway as in normal sinus rhythm. Abbreviations are the same as those in Figure 2.

**Figure 8.** SAN reentry induced depression of excitability near conduction pathways and exit block. **(A)** Longitudinal conduction block (LB) and SAN slow-slow micro-reentry (R1 and R2) induced by atrial tachypacing (5 Hz) are shown. Below the ECG recording, dV/dt of the extracted SAN signals are shown for the OAPs selected from the right superior SACP (P) and the neighbor SAN region (1). dV/dt represents a surrogate of the SAN excitability. Note that the values of dV/dt measured during the SAN reentry are smaller than those during sinus rhythm (S1). **(B)** Activation maps and the corresponding dV/dt distribution maps reconstructed for the selected beats. Abbreviations are the same as those in Figure 2.

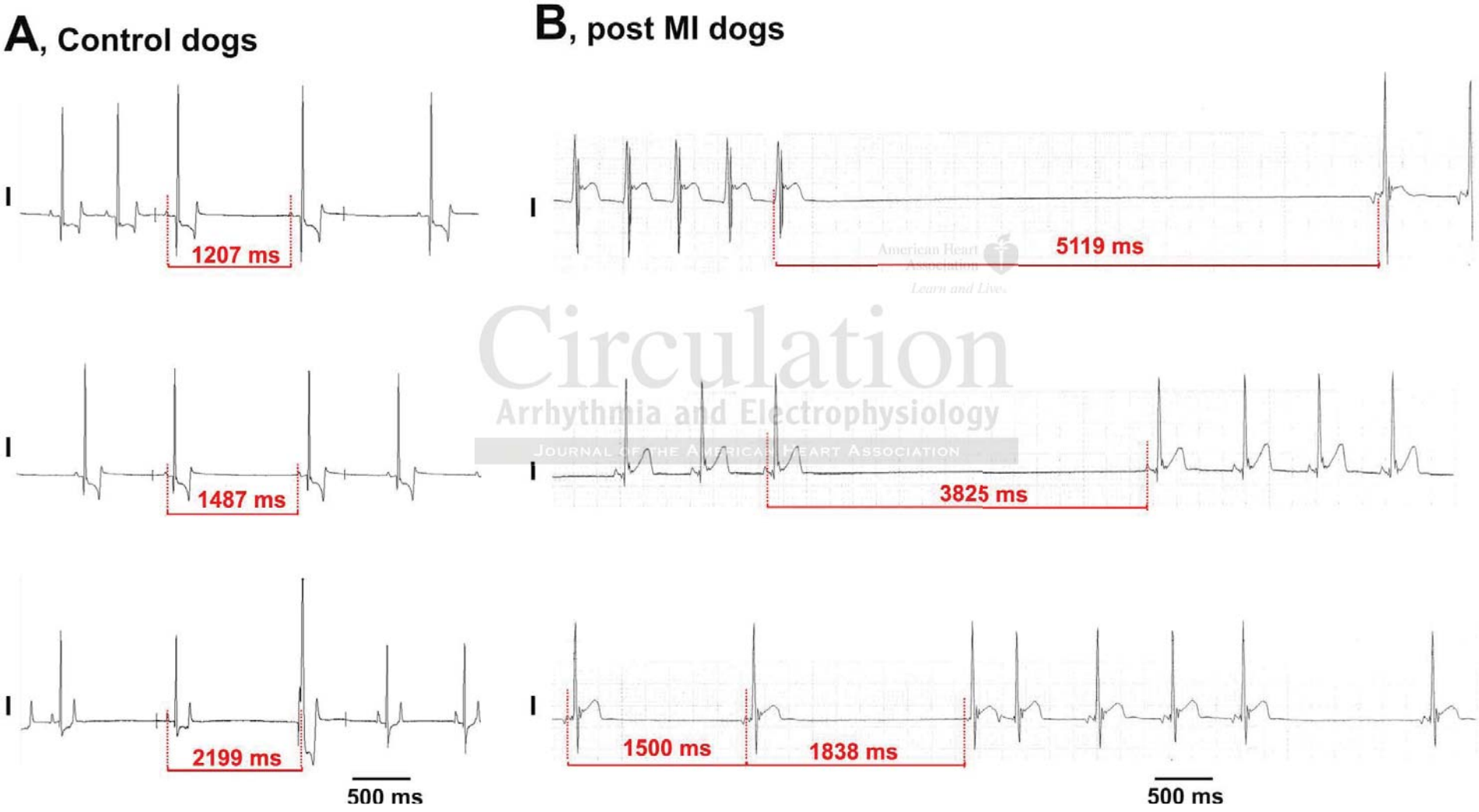

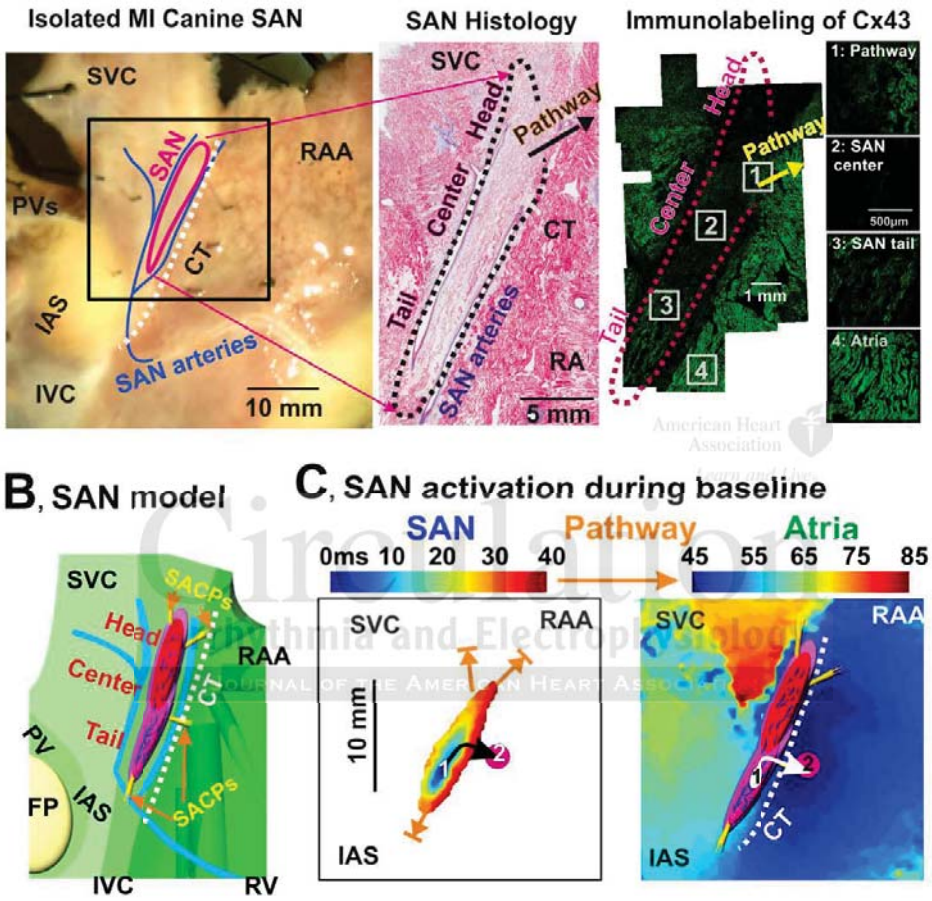
A, Dog#3 SAN pacemaker complex structure
Isolated MI Canine SAN
SAN Histology
Immunolabeling of Cx43
SVC
RAA
PVs
SAN
CT
IAS
IVC
SAN arteries
10 mm
Head
Pathway
Center
Tail
RA
5 mm
1: Pathway
2: SAN center
500μm
3: SAN tail
4: Atria
1 mm
B, SAN model
SACPs
PV
FP
RV
C, SAN activation during baseline
SAN
Pathway
Atria
0ms 10 20 30 40
45 55 65 75 85
10 mm
D
SACT=45ms
OAPs
1-SAN
2-Atria
Extracted SAN OAP
CL (ms):
538
535
535
534
533
Atrial ECG
0.5 sec

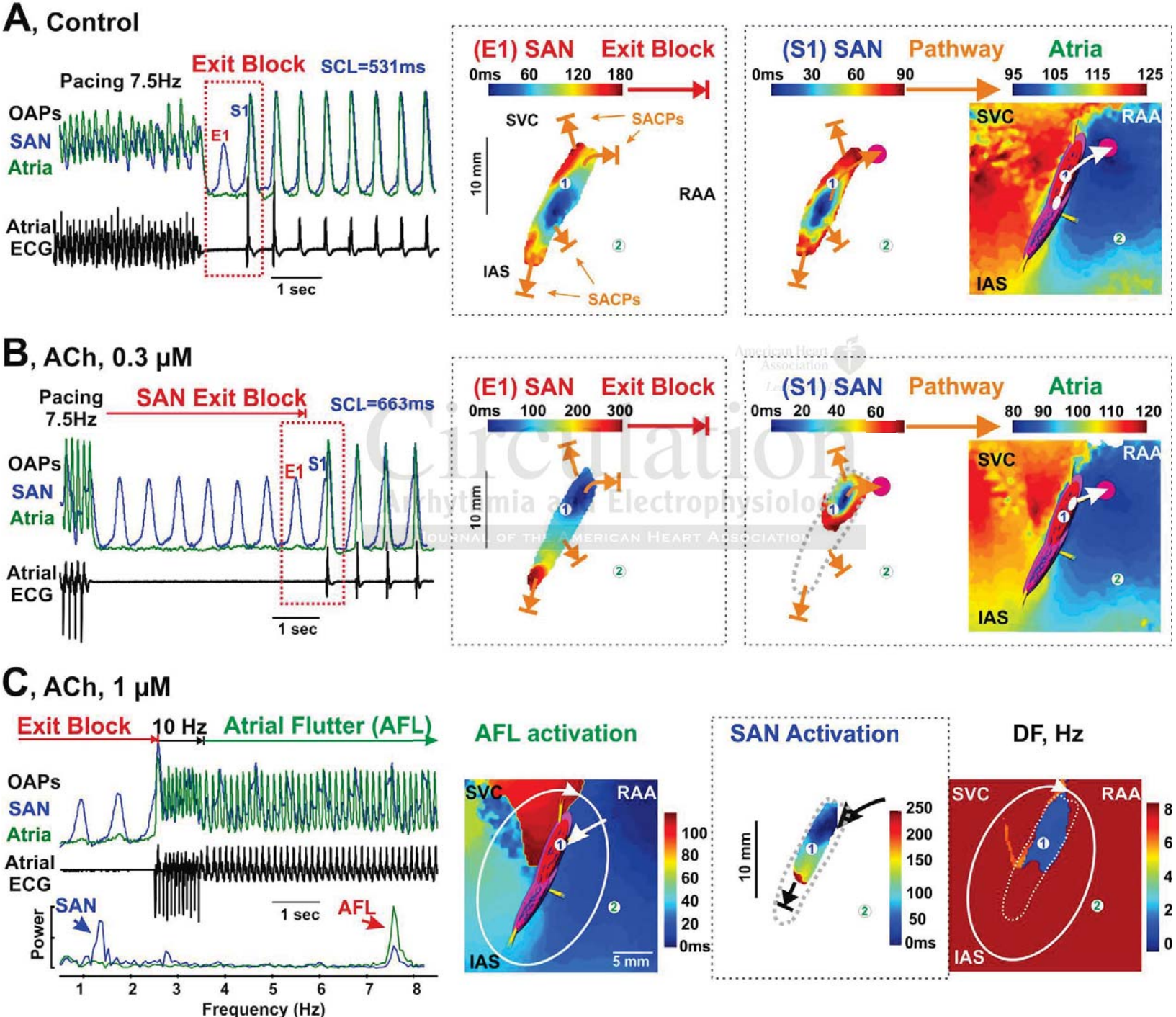

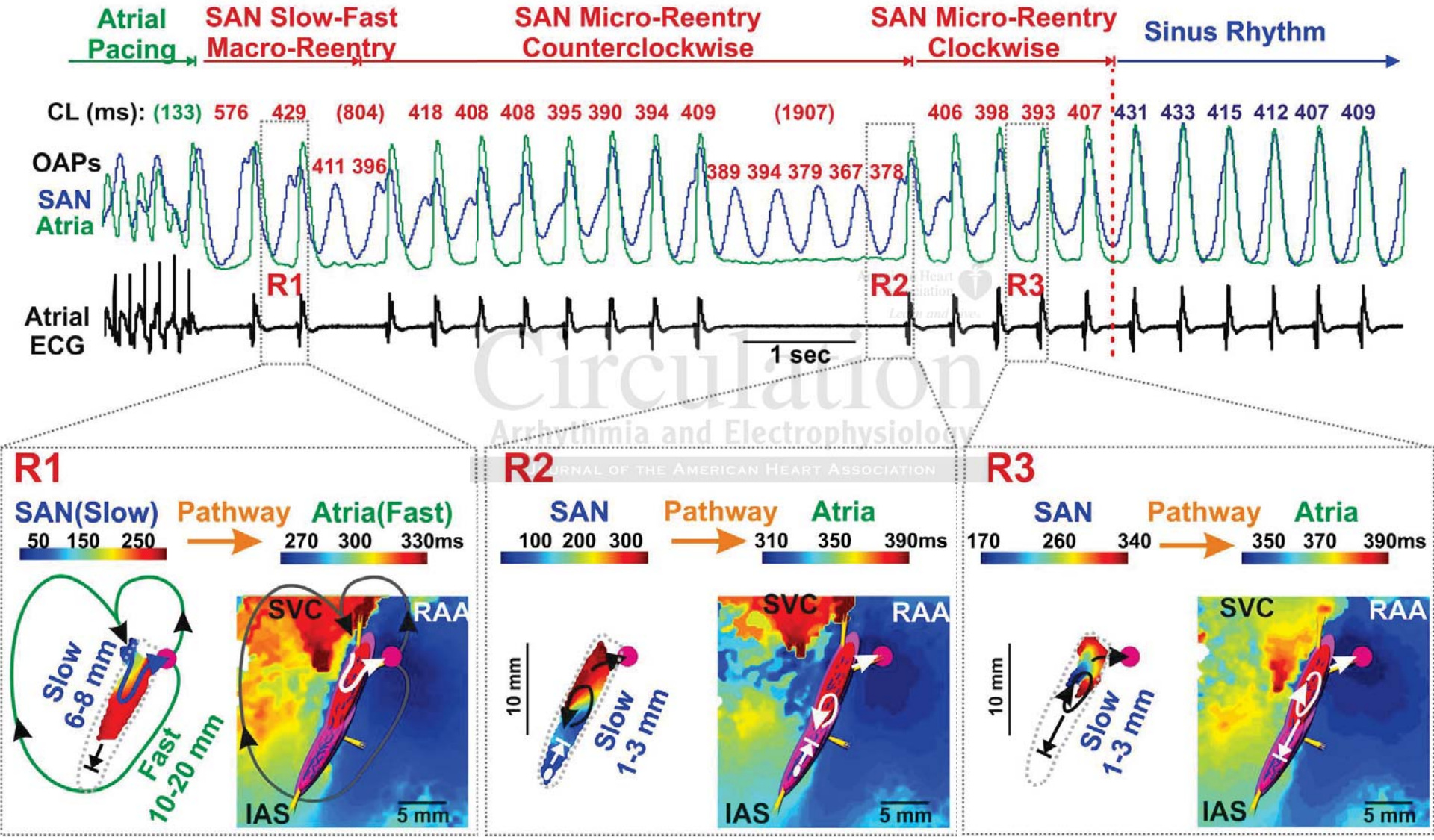
Atrial Pacing
SAN Slow-Fast Macro-Reentry
SAN Micro-Reentry Counterclockwise
SAN Micro-Reentry Clockwise
Sinus Rhythm
CL (ms): (133) 576 429 (804) 418 408 408 395 390 394 409 (1907) 406 398 393 407 431 433 415 412 407 409
OAPs
SAN
Atria
411 396
389 394 379 367 378
R1
R2
R3
Atrial ECG
1 sec
R1
SAN(Slow) Pathway Atria(Fast)
50 150 250
270 300 330ms
Slow 6-8 mm
Fast 10-20 mm
SVC
RAA
IAS
5 mm
R2
SAN Pathway Atria
100 200 300
310 350 390ms
10 mm
Slow 1-3 mm
SVC
RAA
IAS
5 mm
R3
SAN Pathway Atria
170 260 340
350 370 390ms
10 mm
Slow 1-3 mm
SVC
RAA
IAS
5 mm

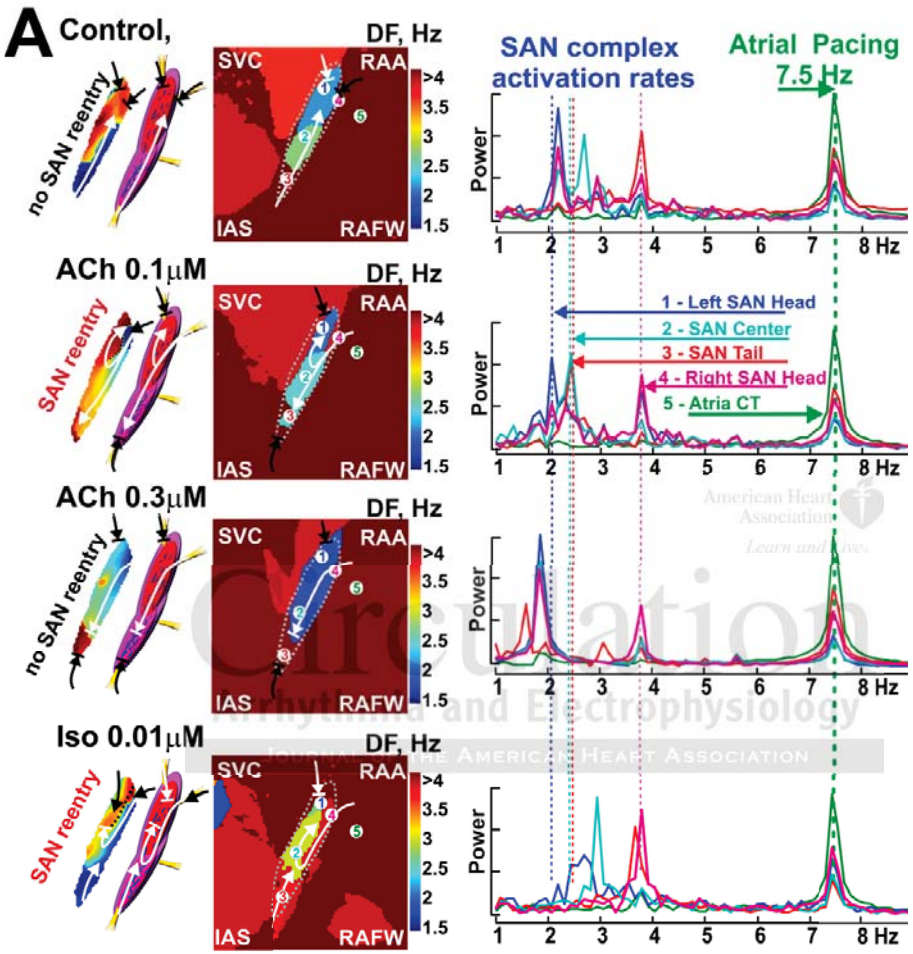


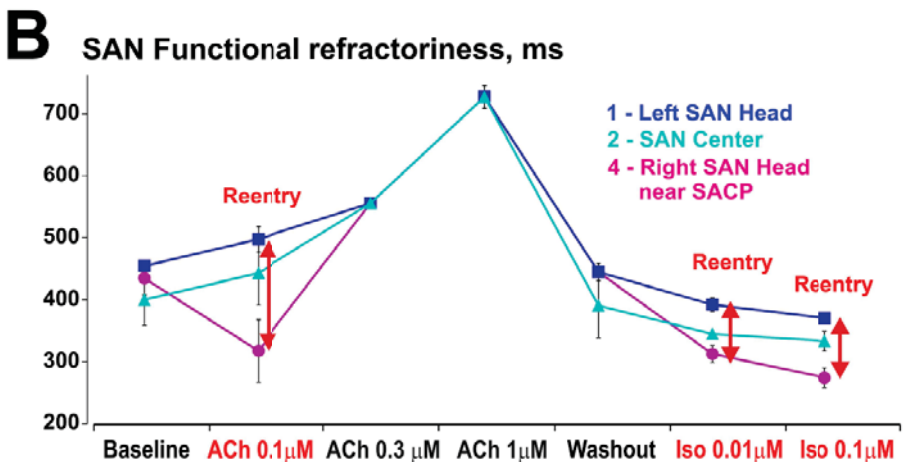

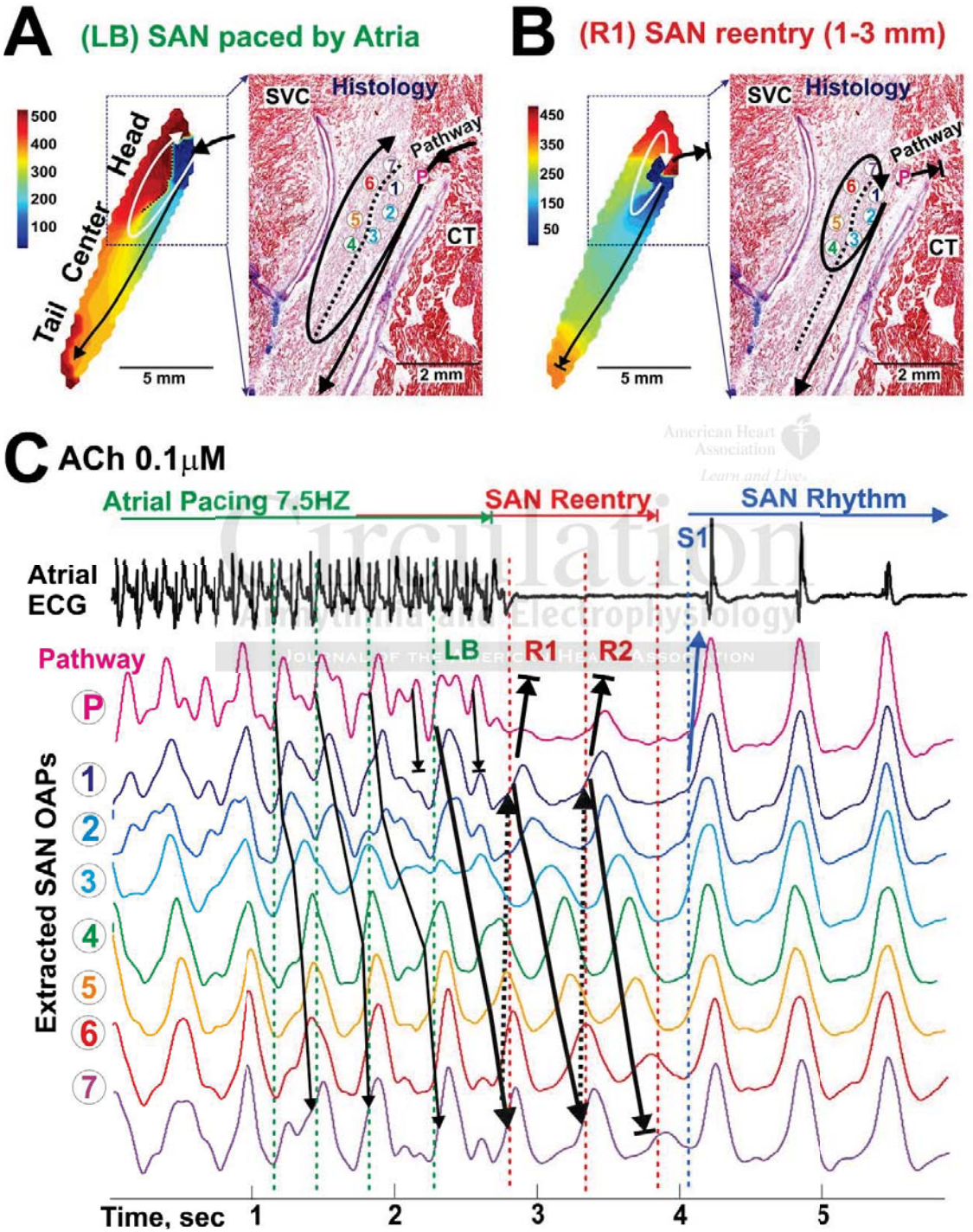
A
(LB) SAN paced by Atria
500
400
300
200
100
Head
Center
Tail
5 mm
SVC
Histology
Pathway
P
CT
2 mm
B
(R1) SAN reentry (1-3 mm)
450
350
250
150
50
5 mm
SVC
Histology
Pathway
P
CT
2 mm
C
ACh 0.1μM
Atrial Pacing 7.5HZ
SAN Reentry
SAN Rhythm
S1
Atrial ECG
Pathway
LB
R1
R2
P
1
2
3
4
5
6
7
Extracted SAN OAPs
Time, sec
1
2
3
4
5

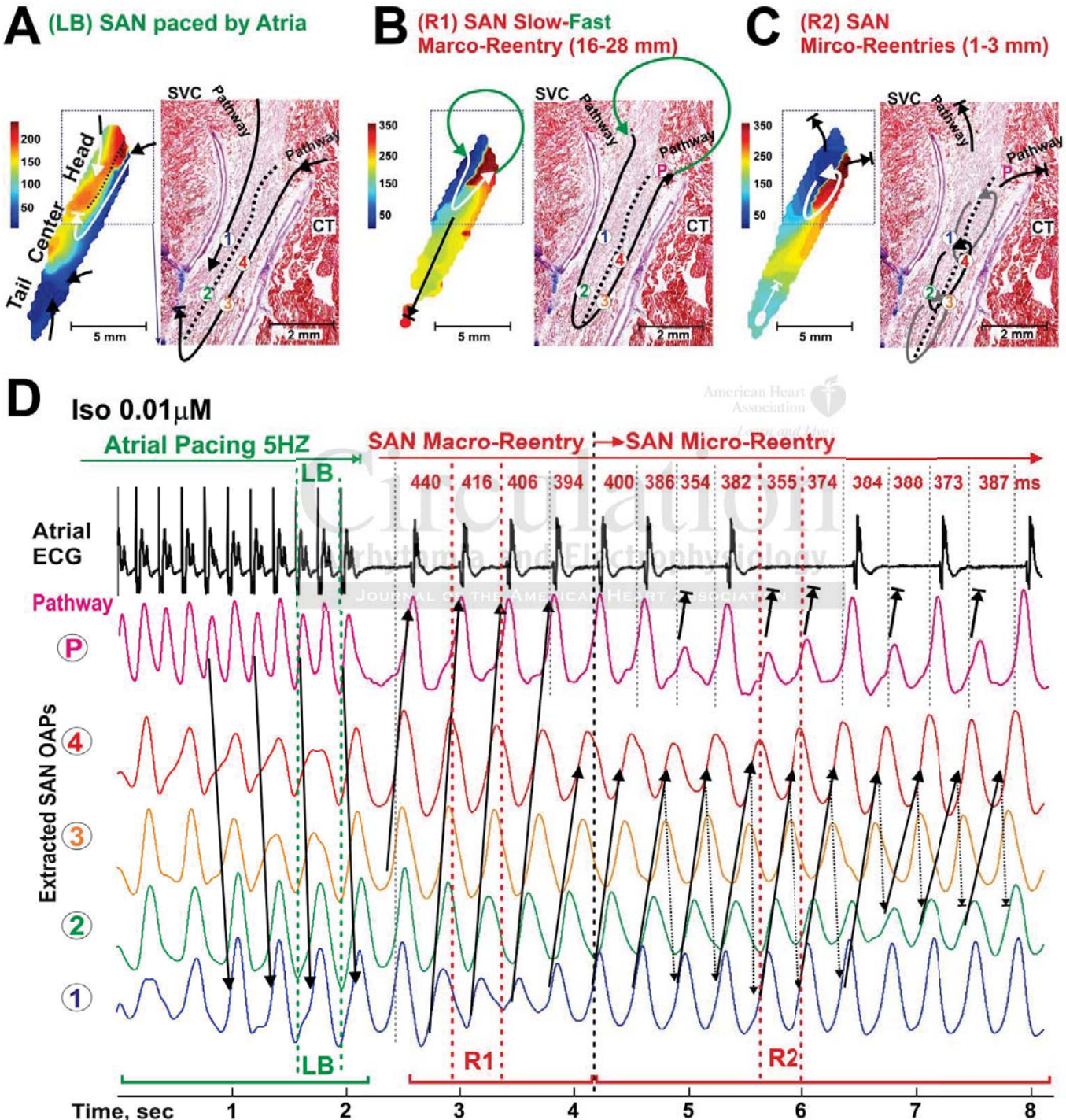
A
(LB) SAN paced by Atria
B
(R1) SAN Slow-Fast
Marco-Reentry (16-28 mm)
C
(R2) SAN
Mirco-Reentries (1-3 mm)
SVC
Pathway
Head
Center
Tail
CT
5 mm
2 mm
D
Iso 0.01μM
Atrial Pacing 5HZ
SAN Macro-Reentry
SAN Micro-Reentry
LB
440 416 406 394 400 386 354 382 355 374 384 388 373 387 ms
Atrial ECG
Pathway
P
Extracted SAN OAPs
4
3
2
1
R1
R2
Time, sec
1 2 3 4 5 6 7 8